TECHNICAL ARTICLE

CrossMark

Influence Analysis of Mining's Effect on Failure Characteristics of a Coal Seam Floor with Faults: A Numerical Simulation Case Study in the Zhaolou Coal Mine

Xiangxi Meng[1] · Weitao Liu[1] · Dianrui Mu[1]

Abstract

A fluid–solid coupled numerical simulation was carried out for the Zhaolou coal mine using Flac3D software. The results showed that: (1) when the failure depth of the floor exceeded the extension depth of the floor rock mass and the hydrostatic seepage pressure of the fractured structure surface exceeded the stress state of the fractured element, floor water inrush will occur. (2) With other factors being equal, if the footwall is mined first, the pore pressure concentration near the fault is more obvious, and the floor-confined water is lifted 10–25 m higher than when the hanging-wall is mined first. Mining the floor adversely affects its plastic zone, and the failure depth is ≈10 m greater than when the hanging wall is mined first. (3) When advancing against the fault dip, the pore pressure concentration near the fault is more obvious, and the floor confined water is lifted 5–20 m higher than when the mine advances along the fault dip. Again, mining the floor first disrupts the floor plastic zone, and the failure depth is approximately 5 m greater than when the mine is advanced along the fault dip. (4) The risk of floor-water inrush is minimized when the hanging-wall is mined first and the mine advances along the fault dip; the risk is greatest when the footwall is mined first and is advanced against the fault dip. These results provide a theoretical basis for preventing mine water inrush.

Keywords Water inrush · Failure depth · Pore pressure · Fracture element stress state

Introduction

As mining depths and intensity have increased, the encountered hydrogeological conditions have become more complicated (Lamoreaux et al. 2014). Therefore, coal-mine floor water inrush accidents have increased year by year. A specific type of inrush is a lagging water inrush in which the water floods into an opening space from aquifers through fractures within the fault zones, usually with a time delay. Such events are a huge threat to the coal mines in China, and

Xiangxi Meng, Weitao Liu and Dianrui Mu contributed equally to the work.

✉ Weitao Liu
  skdlwt@126.com

✉ Dianrui Mu
  1731799913@qq.com

[1] College of Mining and Safety Engineering, Shandong
    University of Science and Technology, Qingdao 266590,
    Shandong, China

difficult to prevent (Wu et al. 2011). There are many factors influencing water inrush from a coal-mine floor, such as the stress of the original rock, the geological structure, and the effects of mining, with fault activation being one of the key factors (Liu et al. 2017; Miao et al. 2004; Wang and Liu 1992; Zhang et al. 1997). However, mining is what activates the faults and induces water to flow along the fractured zone (Lu et al. 2009). Mining affects the secondary stress distribution and deforms and damages the rock to a certain depth below and above the mine (Wu 2007). Multiple factors affect the scale of the problem, such as face size, mining height, mining mode, and geological structure.

Study of excavation-induced water inrush has evolved over the past decades. In general, it is clear that excavation-induced changes in stress and deformation of rock masses can alter the permeability in existing weak structures (e.g. faults, joints, fractures) that are connected to aquifers. In general, a fluid-saturated porous or fractured rock mass can deform due to changes in the external load and the internal pore-fluid pressure (Rutqvist and Stephansson 2003). It is

therefore reasonable to investigate the processes of mining lagging water inrush by considering the coupling between fluids and deformation.

Jiang et al. (2015) studied the evolution of mine stress and the activation of faults during the process of hanging-wall and footwall advancement against the fault dip, and Li et al. (2005) studied the failure of the subsurface aquifer in a similar simulation test. Xu et al. (2012) reported that the necessary condition for water conduction by fault activation should be greater water pressure than normal stress in the original water conduction zone around the fault, according to hydrodynamic theory of fractured media. Jia et al. (2009) analyzed the damage caused by excavation of boom clay influenced by the evolution of pore pressure and plastic strain based on the theory of continuum damage mechanics.

However, this research has been limited to stress analysis; the interaction between the seepage field and the stress field has rarely been considered. Instead, the coal-seam floor stress was studied separately from the confined water. Also, few water inrush studies have studied the effect of mining on fault activation in detail. We studied how mining sequence, fault dip, and the direction mining advancement affected floor rock failures. To carry out the investigation, the Zhaolou coal mine was selected for a research demonstration, and a fluid–solid coupled numerical simulation was carried out using Flac3D software.

Seepage Stress Coupling of the Fractured Rock Mass

Influence of the Seepage Field on the Stress Field of the Fractured Rock Mass

The effect of water flow in fractures affects the mechanical behavior of fracture faces in two ways: the hydrostatic pressure of water flow has a normal expansion effect on the fracture surface, while the flow of the water has a tangential extension effect on it. When a fracture is unfilled (i.e. fractures are open), the tangential force of fracture water on fracture structure is as follows:

$$\tau_w = -\frac{1}{2}\rho g b \frac{\partial h}{\partial x}, \tag{1}$$

where τ_w is the tangential force of fracture water flow to the fracture structure (in MPa); ρ is the density of fracture water (in kg m^{-3}); g is the gravitational acceleration (in m s^{-2}); b is the fracture width (in m), h is the total seepage head (in m); and $\partial h/\partial x$ is the hydraulic gradient of fracture flow along the x direction. At the same time, the normal force on the unfilled fracture is:

$$\sigma_w = \rho g(h - z), \tag{2}$$

where σ_w is the infiltration hydrostatic pressure of fracture surface (in MPa); h is the height of the water level (in m);

and z is the potential head (in m); other parameters have the same meaning as above.

Influence of the Stress Field on the Seepage Field in Fractured Rock

According to the cubic theorem of single-fracture seepage, the single width flow of the joint rock mass is:

$$q = \frac{\gamma b^3 J_f}{12u} \tag{3}$$

where q is the single width flow of the joint rock mass; γ is the bulk density of fracture flow (in N m^{-3}); b is the fracture width (in m); u is the dynamic viscosity coefficient of fracture flow (in N s m^{-2}); and J_f is the hydraulic gradient of fracture flow. It was assumed that the fluid flow in the hydraulic fractures was laminar flow between two parallel plates, and the shape of the fracture was oval (Yuan et al. 2012). The pressure drop equation is:

$$\begin{cases} p = -\dfrac{12uqz}{h_f w_0^2 w} + p_0, \; p \geqslant \sigma_s \\ p = \sigma_s, \; p < \sigma_s \end{cases} \tag{4}$$

Combining Eq. (3) with Eq. (4), the pressure-drop equation in a single-fracture structure is:

$$\begin{cases} p = -\dfrac{\gamma z b^3}{h_f w_0^2 w} + p_0, \; p \geqslant \sigma_s \\ p = \sigma_s, \; p < \sigma_s \end{cases} \tag{5}$$

where h_f is the fracture depth (in m); w_0 is the widest width of the fracture (in m); w is the width of the fracture at any position (in m); p_0 is the aquifer water pressure of the floor (in MPa); σ_s is the closed stress of the fracture surface (in MPa); and other parameters have the same meaning as above.

As can be seen from Eq. (5), after floor mining, the deeper that fractures penetrate near the fault zone above the Ordovician limestone aquifer, the greater the pore pressure in the fracture, and the higher the water will be lifted along the fault zone, increasing the risk of water inrush.

Mechanical Analysis of a Floor Water Inrush

Single-Fracture Extension Mechanics Model

Based on the mechanism of fluid–solid coupling, the hydrodynamic pressure generated by water flow in an open fracture causes shear structural extension, which can further

extend the length of the fracture structure in the permeation direction. According to elastic mechanics, a single-fracture extension mechanics model and force-state diagram of a single-fracture split tetrahedron is established, as shown in Figs. 1 and 2.

In the figures, σ_1, σ_2, and σ_3 are the maximum, intermediate, and minimum principal stresses of the body element in the coal-seam floor, respectively (in MPa); σ_w is the normal expansion force of fracture flow on the fracture, τ_w is the tangential force of fracture flow on the fracture surface (in MPa), σ'_n is the normal expansion force of the separating element body to the fracture when stress-seepage coupling occurs in the fractured rock mass; τ'_n is the tangential force of the separating element body on the fracture when stress-seepage coupling occurs in the fractured rock mass (in MPa); σ_n is the normal expansion force of the separating element body on the fracture regardless of the fluid–solid–coupling effect of the fractured rock mass; and τ_n is the tangential force of the separating element body on
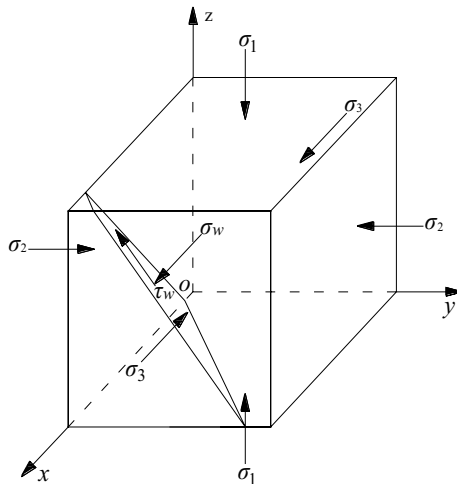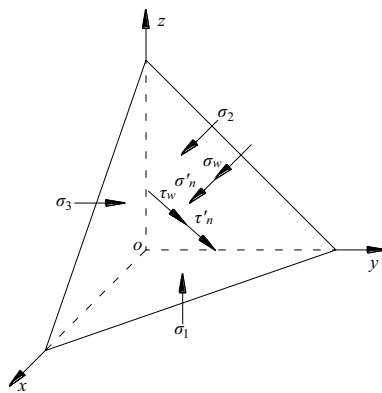
the fracture regardless of the fluid–solid–coupling effect of the fractured rock mass (in MPa).

According to the theory of elasticity mechanics (Chen et al. 1977; Shen et al. 2014; Xu et al. 2007), considering the fluid–solid–coupling effect of the fractured rock mass, the force of the separation element on the fracture surface is:

$$
\begin{cases}
\sigma'_n = l^2\sigma_1 + m^2\sigma_2 + n^2\sigma_3 + 2mn\tau_{yz} \\
\qquad + 2nl\tau_{zx} + 2ml\tau_{xy} - \sigma_w \\
\tau'_n = [(l\sigma_1 + m\tau_{yx} + n\tau_{zx})^2 + (m\sigma_2 + n\tau_{zy} + l\tau_{xy})^2 \\
\qquad + (n\sigma_3 + l\tau_{xz} + m\tau_{yz})^2]^{1/2} - \tau_w
\end{cases}
\tag{6}
$$

where m is the cosine of the fracture-plane normal vector and the direction of the x axis; n is the cosine of the fracture-plane normal vector and the direction of the y axis; l is the cosine of the fracture-plane normal vector and the direction of the z axis; τ_{xy}, τ_{xz}, and τ_{yz} are the respective shear-stress components on the coordinate plane (in MPa); and the other parameters have the same meaning as above.

A change in the permeability of a rock mass is the essence of water inrush. Stress-seepage three-axis rock experiments have shown that the fracture structure is closed under the effective stress of a detached element (that is, $\sigma'_n \neq 0$ and $\tau'_n \neq 0$). Although the fracture has been formed, the permeability of the rock does not increase. Instead, it decreases as stress increases, and the jump point of its permeability is delayed to the strain softening stage after the stress peak, according to Zhang and Pang (2010). Therefore, the expansion and penetration of a jointed rock fracture may not lead to a sudden increase in rock permeability; the relationship between the stress state of a fractured rock mass and the strong seepage of confined water is the key to any sudden jump in permeability. When the hydrostatic pressure of the confined water and the tangential force of the confined water flow to the fissure wall is greater than the effective stress of the separation element on the fracture surface, changes in rock mass permeability can occur. According to Griffith's strength theory, the fracture expansion of a jointed rock mass is mainly caused by the normal expansion of confined water; and the tangential force of seepage is less obvious and can be ignored. Therefore, the general condition for the permeability mutation of a fractured rock mass under stress-seepage coupling is:

$$
\sigma_w > \sigma_1 l^2 + \sigma_2 m^2 + \sigma_3 n^2 + 2(mn\tau_{yz} + nl\tau_{zx} + ml\tau_{xy})
\tag{7}
$$

Fig. 1 Mechanical model of fracture extension

Fig. 2 Segmentation tetrahedral stress state of fracture

Mechanics Criterion of Floor Water Inrush

The existing theories and exploration methods make it difficult to accurately predict and explore the expansion of

fracture rock because the development, expansion, and trans-fixion location of floor fractures are complicated. Therefore, Zhang and Pang (2010) established the maximum failure depth calculation formula of horizontal coal seam floor based on elastic theory, which can be applied to calculate the expansion and transfixion depth of floor fractures:

$$h_f = \frac{(k+1)H}{2\pi}(\cot \varphi_0 - \frac{\pi}{2} + \varphi_0) - \frac{C}{\gamma \tan \varphi_0} - H_m \quad (8)$$

where h_f is the penetration depth of the floor (in m); k is the support pressure concentration factor of the lateral face, H is the depth of the coal seam (in m); ϕ_0 is the average internal friction angle of the coal-seam floor (in deg); C is the average cohesion of the coal-seam floor (in MPa); γ is the average bulk density of the coal seam floor (in N m^{-3}); and H_m is the caving height (in m).

A number of rock specimen uniaxial compression tests have shown that only specimen with less than a 60° angle between the fracture and the axial compressive stress can develop a regular crack extension, and that the fracture structures of other specimens are not extended along the original crack direction in uniaxial compression tests with different inclination initiation cracks. Therefore, if the angle between the fracture-damage surface direction and the maximum principal stress (σ_1) direction is 0°, while the angles between the fracture-damage surface direction and the intermediate stress direction (σ_2), minimum principal stress (σ_3) directions are both 45°. In this case, in Eq. (7), $l = 0$, $m = n = \sqrt{2}/2$, Combining Eq. (2) with Eqs. (7, 9) is derived,

$$\rho g(h - z) > (\sigma_2 + \sigma_3)/2 + \tau_{yz}. \quad (9)$$

Combining Eq. (8) with Eq. (9), the mechanical criterion of water inrush in the mine floor is derived:

$$\begin{cases} h_f = \frac{(k+1)H}{2\pi}(\cot \varphi_0 - \frac{\pi}{2} + \varphi_0) - \frac{C}{\gamma \tan \varphi_0} - H_m gt; h_{\text{up}} \\ \sigma_w = \rho g(h - z)gt; (\sigma_2 + \sigma_3)/2 + \tau_{yz} \end{cases}$$
$$(10)$$

where σ_2 is the intermediate principal stress of pressure relief floor of the goaf (in MPa); σ_3 is the minimum principal stress of pressure relief floor of the goaf (in MPa); h_{up} is the lifting distance between coal seam and floor confined water (in m), which can be determined by the existing detection methods; and the other parameters have the same meaning as above.

Based on this analysis, the risk of a floor water inrush is related to the failure depth in the floor, the confined water pressure, and the stress of the fractured unit caused by the mining. Therefore, even if the failure depth of floor caused by the mining is greater than the thickness of the floor

aquifuge, floor water inrush will not necessarily occur. Only if the floor fracture penetration depth and the stress state of fractured unit caused by the mining have met the above-mentioned condition at the same time will a coal seam floor water inrush occur.

Numerical Simulation of Floor Mining Failure

Engineering Background

The average elevation of the 11,301 working face, which is located in the southeast part of the Zhaolou mine, is +42.9 m; the average elevation of the downhole is −921.3 m; the thickness of the coal seam is 6.5 m; the length of the working face is 270 m; and the width of the tilt is 190 m. The geological structure of the face is complicated and there are five combined faults: FD13, F11103, F11102, F11104, and F11106. Among these, there are two faults with a fall head of 5~10 m and three faults with a fall head of less than 5 m. FD13 is a normal fault with a fall head of 9 m, the fault dip is 70°, extending 373 m in the working face, which greatly affects the mining.

Numerical Simulation

Using the mining conditions of the 11,301 working face as an example, a numerical model was established based on the constitutive model of Mohr–Coulomb mechanics (Fig. 3). The lengths of the model's x, y, and z axis are 350, 300, and 260 m respectively, with a total of 178,500 units and 188,292 nodes. The working face in the model adopts long-wall step excavation, and on both sides of the working face
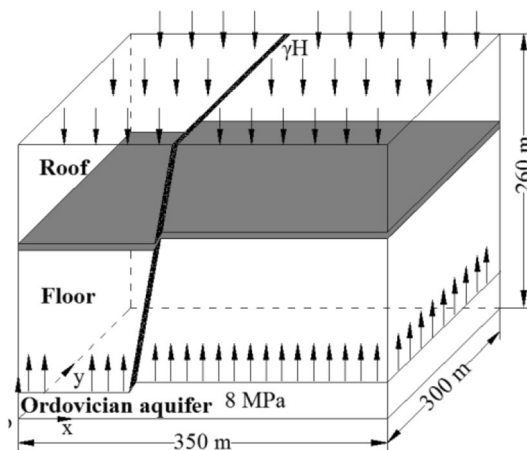
**Fig. 3** Numerical calculation model of confined water coal mining

Table 1 Rock mechanics parameters of the coal-seam roof and floor rocks

Stratum	Density (kg/m³)	Volume modulus (GPa)	Shear modulus (GPa)	Cohesion (MPa)	Strength of extension (MPa)	Internal friction angle (°)	Permeability coefficient (cm/s)	Porosity
Kern stone	2300	5.0	4.8	4.7	4.2	42	3e−13	0.8
Sandstone2	2400	4.1	2.4	3.6	1.8	35	4e−14	0.5
Mudstone2	2200	3.5	2.5	2.3	2.9	32	1e−23	0.2
Sandstone1	2200	2.5	2.2	2.1	3.1	26	1e−22	0.5
Siltstone	2400	3.8	2.5	3.2	2.1	34	2e−15	0.3
Coal seam	1500	2.7	3.6	2.1	2.3	30	2e−16	0.4
Post stone	2200	3.1	2.3	2.2	3.2	28	2e−6	0.3
Sandy mudstone	2200	3.8	2.1	2.1	2.2	29	4e−14	0.3
Mudstone 1	2050	2.2	2.5	2.2	2.8	25	3e−7	0.4
Limestone	2450	4.8	3.8	2.8	3.2	38	9e−7	0.5
Mesograin Sandstone	2250	4.9	3.0	3.7	3.3	38	1e−14	0.6
Fag sandstone	2200	5.2	4.3	4.5	3.8	40	2e−13	0.8
The aquifer in Ordovician limestone	2600	5.1	6.9	6.8	7.1	31	4e−16	0.7

40 m protective coal pillars remain. Each step along the coal seam excavates 15 m, totaling 16 excavation steps to move the face forward 240 m. The boundary conditions of the front, back, left, and right are fixed along the x and y direction, and the bottom is the entire boundary. The top boundary of the model is equivalent to the upper-layer weight of the rock mass with a certain load; a calculated surface force of 9 MPa was applied at the top. The seepage boundary conditions were defined as: the bottom adopts a constant water pressure to simulate the confined water value of the Ordovician limestone aquifer. The initial water pressure of the floor changes according to the gradient water pressure and the rest are watertight boundaries. The goaf is the drainage boundary after the working face mined. The water in the goaf is not considered, and the constant water pressure at the boundary is 0. The rock mechanics parameters of the coal seam roof and floor rocks are shown in Table 1.

Four sets of mining models were designed in this simulation, with 24 monitoring points (Fig. 4). Six monitoring points were set up 10 m under the floor of the hanging-wall working face of the coal seam, with each adjacent two monitoring points spaced 15 m apart. Twelve monitoring points were set up under the working face floor of the hanging wall on the coal seam 10 m at the horizontal position, with each adjacent two monitoring points spaced 15 m apart. 6 monitoring points were set up along the fault dip.

In the figures, a is hanging wall mining first, footwall mining later, advancing along the fault dip; b is hanging-wall mining first, footwall mining later, advance against the fault dip; c is footwall mining first, hanging-wall mining
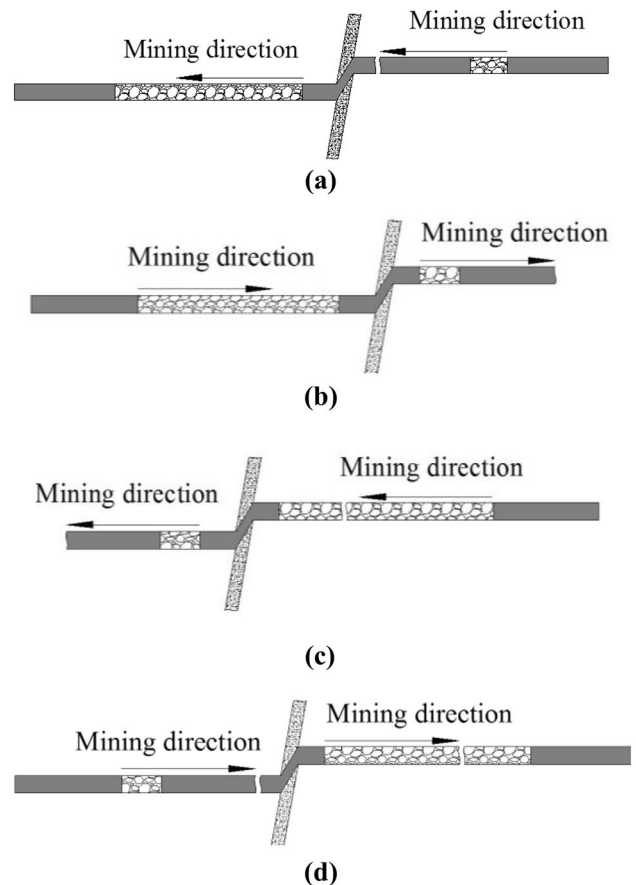
Fig. 4 Schematic models of fault dip and mining sequence

later, advancing along the fault dip; d is footwall mining first, hanging-wall mining later, advancing against the fault dip.

Discussion

Analysis of the Floor Plastic Zone along the Working Face

The distribution cloud pictures of the floor plastic zone along the working face using the devised simulation scheme were obtained (Fig. 5). From the four groups of cloud pictures, the following conclusions can be drawn:

1. After mining, the depth of the plastic failure zone in the four mining models is h_a=30 m, h_b=35 m, h_c=40 m, and h_d=45 m, respectively. It can be seen that when the footwall is mined first and the hanging wall later, mining has a greater influence on the floor's plastic zone. This is because the hanging-wall is closer to the aquifer than the footwall, and the effect of the confined water on the mine floor is obvious.
2. When the mining sequences are the same, advancing against the fault dip can increase the failure depth of the plastic zone, because this produces both lateral andh longitudinal extension destruction in the fault. In addition, to a certain extent, the rock mass on both sides of the fault is destroyed.
3. After mining, the plastic zone of the coal seam roof and floor is mainly affected by shear failure. When the hanging wall is mined first and the footwall later, the failure range of the plastic zone of the coal seam roof is uniform, and advancing against the fault dip can slightly increase the failure range of the roof's plastic zone. When the footwall is mined first and the hanging wall later, the plastic zone of the roof is roughly "saddle shaped", and advancing against the fault dip increases the failure range of the roof plastic significantly compared to advancing along the fault dip. This is because advancing against the fault dip concentrates the pressure on the advance supports, while the upper part of the fault zone impedes mine pressure transmission, which exacerbates the damage to the upper part of the fault zone and the nearby roof.

Analysis of the Floor Pore Pressure Advance

Distribution cloud pictures of the floor pore pressure along the working face according to the devised simulation scheme show the different effects of mining (Fig. 6). Two basic phenomena underlie the poroelastic behavior: solid-to-fluid coupling occurs when a change in applied stress
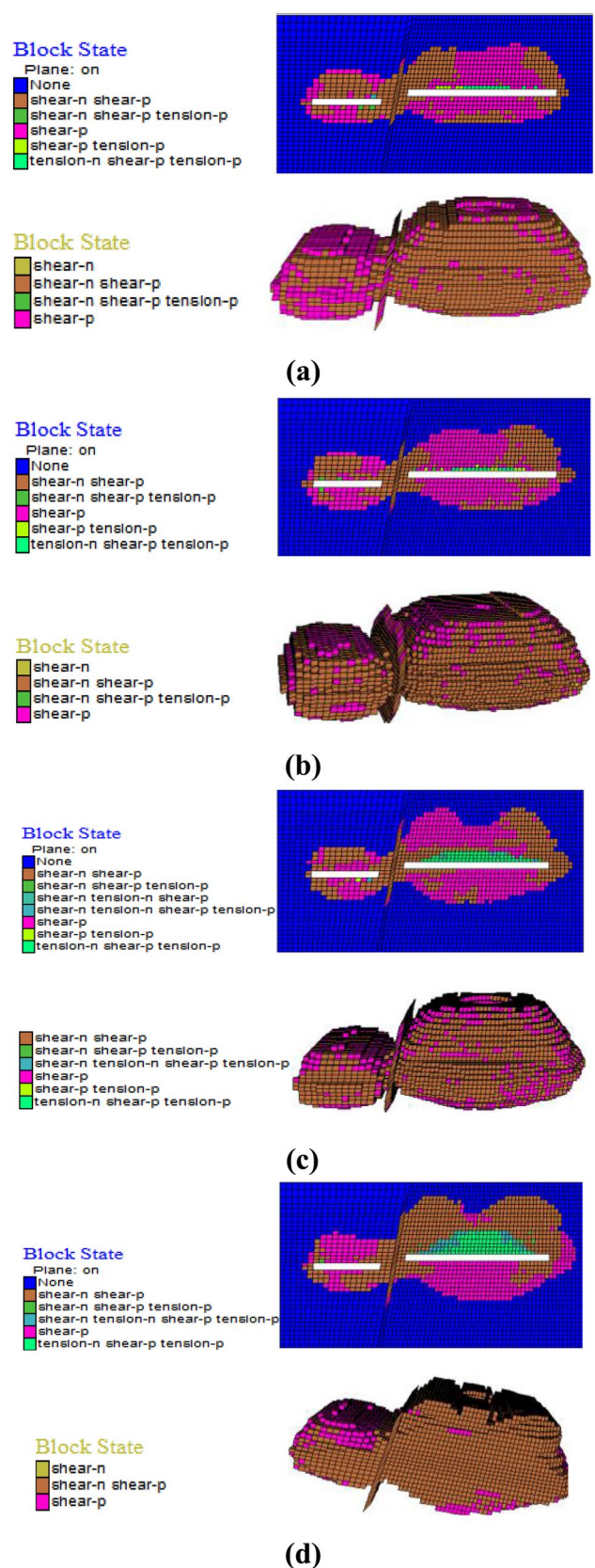

Fig. 5 Cloud pictures of the floor plastic zone in different mining effects

initial pore pressure

(a)

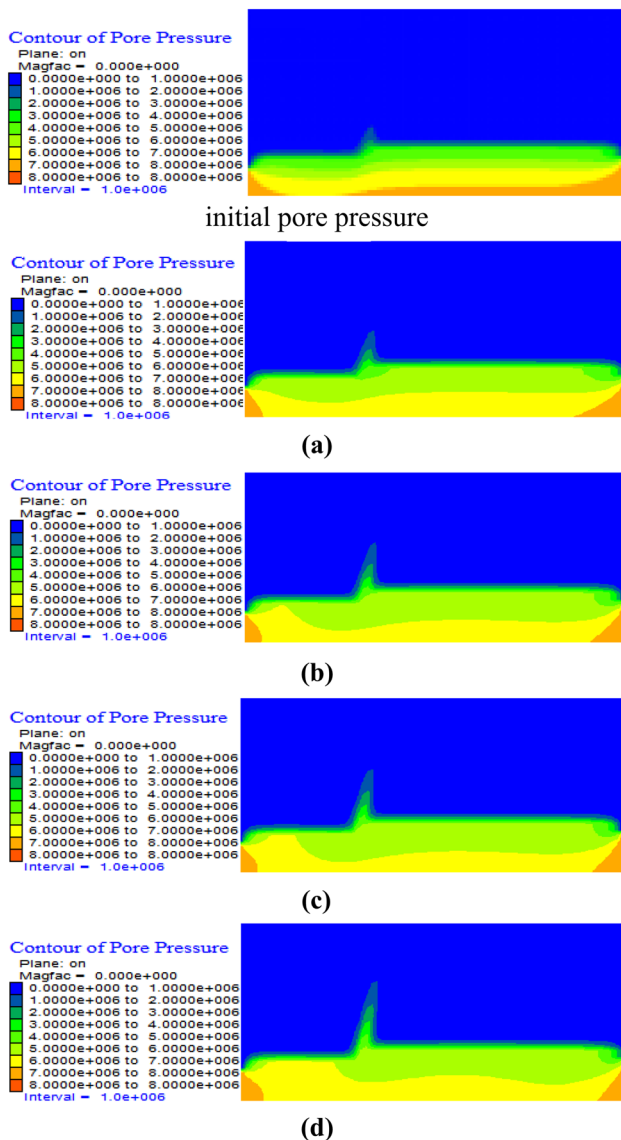
(b)

(c)

(d)

Fig. 6 Distribution cloud pictures of the floor pore pressure in different mining effects

produces a change in fluid pressure or fluid mass. Fluid-to-solid coupling occurs when a change in fluid pressure or fluid mass produces a change in the volume of the porous material (Wang 2000). In the FLAC3D numerical simulation, the variables describing fluid seepage in porous media are the three components of pore pressure, saturation, and specific drainage. The equations relate strain and fluid-mass changes to stress and fluid-pressure changes. After setting CONFIG fluid in the calculation command, the simulation state is seepage mode. The pore pressure changes with the the infiltration line. Solid-to-fluid coupling in the FLAC3D simulation included two aspects: relative time scales can be estimated by the ratio between the coupling process and the

feature time of the non-draining process, and the characteristic time of the undrained mechanical process can be obtained using saturated mass density and undrained volume. Pore pressure is set by INITIAL or PROPERTY commands. In the Flac3D simulation, effect stress, diffusivity, fluid to solid coupling, and specific storage can be set with an INITIAL or PROPERTY command.

The following conclusions can be drawn from the four groups of distribution cloud pictures of the floor pore pressures along the working face:

1. Before the working face is mined, the height of the original conducting zone is 15 m, which is above the Ordovician limestone aquifer and near the fault. The initial pore pressure is substantially layered vertically, and the pore pressure of the lower slice of the aquifer presents a tendency to decrease from both sides to the middle. Since the hanging wall is closer to the aquifer, the confined water has a greater effect on the coal pillar. Therefore, the pore pressure of the lower slice of the aquifer decreases faster.

2. After mining, stress is concentrated on both sides of the lower slice of the aquifer, and the relationship of the lifting heights of the aquifer near the fault are: $h_a = 35$ m, $h_b = 40$ m, $h_c = 45$ m, and $h_d = 65$ m. It can be seen that when the hanging-wall is mined first and the footwall later, the lifting height of the floor-confined water advance along the fault dip is more obvious. This is because, when the footwall is mined first, the rock mass near the fault releases stress, and fault reactivation caused by mining leads to the obvious increase in permeability.

3. When the mining sequences are the same, advancing against the fault dip causes the floor-confined water to rise along the direction of the fault, and increases the fault's seepage pressure. This is because advancing along the fault dip mainly causes longitudinal extension destruction of the fault zone, while advancing against the fault dip causes both longitudinal and lateral extension destruction of the fault zone. In addition, the rock mass on both sides of the fault is destroyed to a certain extent, which increases the permeability of the fault and the rock.

4. The pore pressure variation curve of each monitoring point at 10 m under the coal seam floor are shown in Fig. 7. It can be seen that in the four sets of mining models, the relationship of the seepage pressure of the fault is as follows: $sp_d > sp_c > sp_b > sp_a$. That is, when the mining mode is "a", the seepage pressure of the head at the same position is the smallest. While the mining mode is "d", the seepage pressure of the head at the same position is the largest.
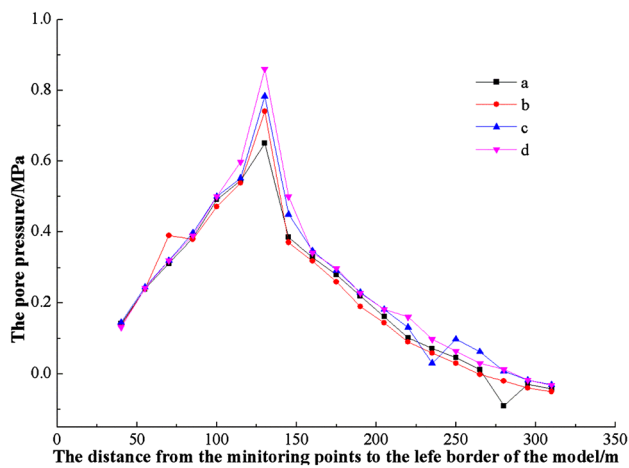
Fig. 7 Pore pressure variation curve of each monitoring point

Analysis of the Stress State of Fractured Floor Rock Mass

The stress states of the fractured rock mass along the working face was obtained for the different mining effects as distribution cloud pictures of $(\sigma 2 + \sigma 3)/2 + \tau yz$ (Fig. 8).

After the working face is mined, the fractured floor of the goaf is in a state of discharging. The stress relief range of the four types of fractured rocks is: $r_d > r_c > r_b > r_a$. The rock mass near the goaf has various degrees of stress concentrations, and the stress peaks are, respectively: $peak_a = 3.88$ MPa, $peak_b = 3.75$ MPa, $peak_c = 3.28$ MPa, and $peak_d = 3.19$ MPa. It can be seen that when the mining mode is "a", the stress state of the fractured rock mass in the goaf is minimized, while when the mining mode is "d", the stress state of the fractured rock mass in the goaf is most affected.

Hazard Analysis of the Floor Water Inrush

The simulation results show that when the mining mode is "d", the mining damage of the floor and the transfixion depth of the coal-floor fracture and the seepage pressure of the floor-confined water are all maximized. In addition, the stress state of the fractured rock mass in the goaf is most affected by the mining, and its stress peak is a minimum. Therefore, when the mining mode is "d", a water inrush of the floor is more likely to occur, since the fracture penetration depth of the floor is greater than the thickness of the aquifer, and the seepage pressure of the confined water exceeds the stress peak of floor fractured rock mass. According to the water inrush criteria, the relationship of the floor water inrush risk is: $risk_d > risk_c > risk_b > risk_a$.
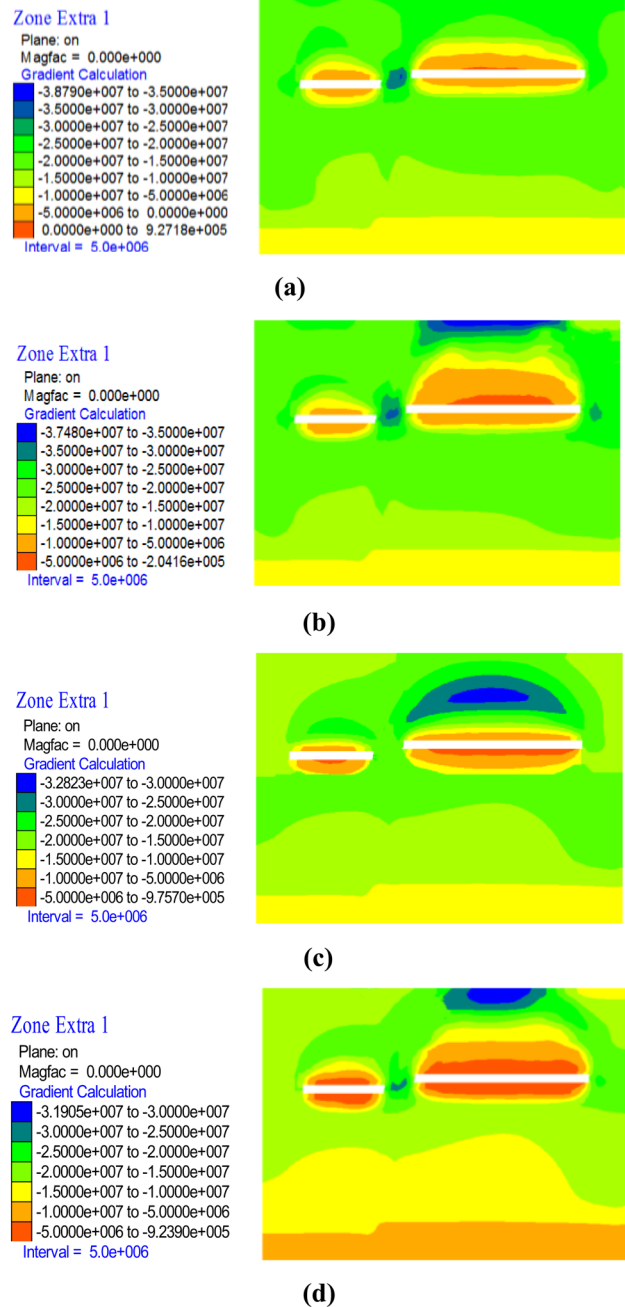

Fig. 8 Floor fractured rock mass stress state cloud pictures

Prevention of Water Inrush

For the high Ordovician confined water layer, dewatering of the area is very necessary for safe mining. Dewatering can reduce the water level to the mining level or make the confined water pressure less than the mechanical strength of the aquifer, which makes mining safe. The Zhaolou coal mine is a basic enclosed hydrogeological unit, while the three grey aquifer and Ordovician limestone are water-filled aquifers.

The confined water of the coal seam floor is the main water source, and fractures in the floor and a small fault are the main water inrush channels. There was no substantial change in the supply and recharge conditions of the mine for several years, as the mine was dewatered. Due to the limited volume of water, the well-developed fractures, and the good connectivity, dewatering of the mine area was relatively easy. In addition, a dewatering experiment conducted in the early stage of the construction well, found that the karst in the mining area has good dredging ability. Based on that, dewatering of the mine area is main water control technology in the Zhaolou mine. The working face has been arranged with a large number of dewatering and dewatering holes, and there are six dewatering pumps in the dewatering roadway. The combined dewatering capacity is at least 580 m^3/h. After years of dewatering, the water level of the limestone has decreased greatly, and mining have preceded safety.

Conclusions

1. A floor water inrush model was established and the floor water inrush criteria were derived. When the failure depth of floor exceeds the extension depth of the floor rock mass, and the hydrostatic seepage pressure of the fractured structure surface exceeds the stress state of the fractured element, floor water inrush will occur.

2. Assuming the same advancing direction, mining the footwall first increases the pore pressure near the fault and the floor-confined water can be lifted 10–25 m higher than when the hanging-wall is mined first. The floor mining is more destructive to the floor's plastic zone, and the failure depth is ≈ 10 m greater than when the hanging wall is mined first.

3. When the sequence of mining is the same, advancing against the fault dip increases the pore pressure near the fault, and the floor-confined water can be lifted 5–20 m higher than when advancing along the fault dip. Again, floor mining is more destructive to the floor plastic zone, and the failure depth is approximately 5 m greater than when advancing along the fault dip.

4. The simulation results show that when the mining mode is "a", the risk of floor water inrush is minimal and mining is safer. Using mining mode "d" increases the risk of floor water inrush and therefore, should be used as little as possible.

References

Chen PS, Gu JC, Li WX (1977) Research on earthquake rupture process and earthquake prediction from the point of view of fracture mechanics. Chin J Geophys 20(3):185–202

Jia SP, Chen WZ, Yu HD, Li XL (2009) Research on seepage-stress coupling damage model of boom clay during tunneling. Rock Soil Mech 30(1):19–26

Jiang JQ, Wu QL, Qu H (2015) Characteristic of mining stress evolution and activation of the reverse fault below the hard-thick strata. Coal Sci Technol 40(2):267–277

Lamoreaux JW, Wu Q, Zhou W (2014) New development in theory and practice in mine water control in china. Carbonate Evaporite 29(2):141–145

Li ZH, Zhai CZ, Li FL (2005) Experimental study on water inrush mechanism due to floor faults activation in mining above confined aquifer. J Cent Univ 46(5):1806–1811

Liu WT, Mu DR, Xie XX (2017) Sensitivity analysis of the main factors controlling floor failure depth and a risk evaluation of floor water inrush for an inclined coal seam. Mine Water Environ. https://doi.org/10.1007/s10230-017-0497-6

Lu X, Liu Q, Wu C, Zhao J (2009) Hydro-mechnaical coupling analysis of mining effect around fault fractured zone. Rock Soil Mech 30(S1):165–168

Miao X, Liu W, Chen Z (2004) Seepage Theory of Mining Rock Mass. Science Press, Beijing

Rutqvist J, Stephansson O (2003) The role of hydromechanical coupling in fractured rock engineering. Hydrogeol J 11(1):7–40

Shen JJ (2014) Research on fracture expanding in deep mine and water inrush channel formation mechanism. Shandong Univ of Science and Technology, Qingdao

Wang HF (2000) Theory of linear poroelasticity. Princeton

Wang ZY, Liu HQ (1992) Mining Above Pressure Water. China Coal Industry Publ House, Beijing

Wu J (2007) Coal seam floor effect and rock mass structure of water resistance performance control action research. China Univ of Mining, Xuzhou

Wu Q, Liu YZ, Liu DH, Zhou WF (2011) Prediction of floor water inrush: the application of GIS-Based AHP vulnerable index method to Donghuantuo coalmine, China. Rock Mech Rock Eng 44(5):591–600

Xu ZL (2007) Elastic Mechanics. Higher Education Press, Beijing

Xu JP, Zhang FC, Gui H, Zhang TJ (2012) Characteristics and experimental study of water conduction caused by fault activation due to mining. J China Univ Min Technol 41(3):415–419

Yuan ZG, Wang HT, Hu GZ, Fan XG, Liu NP (2012) Numerical simulation of hydraulic fracturing of crossing borehole and its engineering application. J Chin Coal Soc 37(S1):109–114

Zhang Y, Pang YH (2010) Water-inrush mechanical model based on a theory of coupled stress-seepage. J Chin U Min Tech 39(5):659–664

Zhang J, Zhang Y, Liu T (1997) Rock Mass Permeability and Water Inrush of Coal Mines. Geological Publ House, Beijing